

Vortex particle simulations of aircraft wake instabilities on massively parallel architectures

Philippe Chatelain¹, Alessandro Curioni², Michael Bergdorf¹, Diego Rossinelli¹, Wanda Andreoni², and Petros Koumoutsakos¹

¹ Computational Science and Engineering Laboratory
ETH Zurich, CH-8092, Switzerland

Phone: +41 44 632 7159

Fax: +41 44 632 1703

² Computational Biochemistry and Material Science group
IBM Research Division - Zurich Research Laboratory
Saumerstrasse 4, CH-8003 Rueschlikon, Switzerland

Phone: +41 44 724 8633

Fax: +41 44 724 8958

Abstract. We present the Direct Numerical Simulations of high Reynolds numbers vortical flows employing vortex methods. The simulations involve a highly efficient implementation on massively parallel computers, enabling unprecedented simulations using billions of particles.

Present results of this work include the investigation of the implementation performance up to 16k IBM BG/L nodes and the study of multiple wavelength instabilities in aircraft wakes, enabling state of the art calculations at high Re numbers. Ongoing developments include simulations using up to 32k processors, the implementation of unbounded conditions and the evolutionary optimization of flow decay and mixing.

1 Introduction

Vortex methods exemplify the computational advantages and challenges of particle methods in simulations of incompressible vortical flows. These simulations are based on the discretization of the vorticity-velocity formulation of the Navier-Stokes equations in a Lagrangian form.

In the recent years hybrid techniques (see [1, 2] and references therein) have been proposed where a mesh is used along with the particles in order to develop efficient and accurate computations of vortical flows.

In this work, we present an efficient and scalable implementation of these methodological advances for the massively parallel architecture of the IBM BG/L. The present results involve DNS on 4k processors and an efficiency investigation going up to 16k processors and 6 billion particles.

The method is applied to the decay of aircraft wakes and vortex rings. The wake of an aircraft consists of long trailing vortices that can subject the following aircraft to a large downwash. Several research efforts have focused on the identification of the governing physical mechanisms of wake evolution that

would lead to design of vortex wake alleviation schemes[3–7]. Flight realistic conditions involve turbulent flows ($Re \sim 10^6$) in unbounded domains for which DNS reference data is still lacking.

State of the art simulations have been limited to low resolution LES in large domains[8], or vortex method simulations[9,10] which achieved $Re=5000$ DNS in short domains and investigated various subgrid stress models for LES in long domains.

The present work enables unprecedented resolutions for the DNS of long wavelength instabilities. The long domain calculation at $Re=6000$ presented herein constitutes the largest DNS ever achieved for a vortex particle method. We also present results for the turbulent decay of a vortex ring at $Re_\Gamma = 7500$. Ongoing work includes simulations at even higher Reynolds on larger partitions of BG/L, the development of unbounded conditions and the coupling of this methodology with evolutionary algorithms in order to accelerate the decay and mixing inside these vortical flows.

2 Methodology

2.1 The remeshed Vortex Particle Method

We consider a three dimensional incompressible flow and the Navier-Stokes equations in its velocity (\mathbf{u})-vorticity ($\boldsymbol{\omega} = \nabla \times \mathbf{u}$) form :

$$\frac{D\boldsymbol{\omega}}{Dt} = (\boldsymbol{\omega} \cdot \nabla) \mathbf{u} + \nu \nabla^2 \boldsymbol{\omega} \quad (1)$$

$$\nabla \cdot \mathbf{u} = 0 \quad (2)$$

where $\frac{D}{Dt} = \frac{\partial}{\partial t} + \mathbf{u} \cdot \nabla$ denotes the Lagrangian derivative and ν is the kinematic viscosity.

Vortex methods discretize the vorticity field with particles, characterized by a position \mathbf{x}_p , a volume V_p and a strength $\boldsymbol{\alpha}_p = \int_{V_p} \boldsymbol{\omega} d\mathbf{x}$. The field is then

$$\boldsymbol{\omega}(\mathbf{x}, t) \approx \sum_p \boldsymbol{\alpha}_p(t) \zeta^h(\mathbf{x} - \mathbf{x}_p(t)) , \quad (3)$$

where ζ is the interpolation kernel and h the mesh spacing. Particles are convected by the flow field and their strength undergoes vortex stretching and diffusion

$$\begin{aligned} \frac{d\mathbf{x}_p}{dt} &= \mathbf{u}(\mathbf{x}_p) , \\ \frac{d\boldsymbol{\alpha}_p}{dt} &= \int_{V_p} (\boldsymbol{\omega} \cdot \nabla) \mathbf{u} + \nu \nabla^2 \boldsymbol{\omega} d\mathbf{x} , \\ &\simeq ((\boldsymbol{\omega} \cdot \nabla) \mathbf{u}(\mathbf{x}_p) + \nu \nabla^2 \boldsymbol{\omega}(\mathbf{x}_p)) V_p . \end{aligned} \quad (4)$$

Using the definition of vorticity and the incompressibility constraint the velocity field is computed by solving the Poisson equation

$$\nabla^2 \mathbf{u} = -\nabla \times \boldsymbol{\omega} . \quad (5)$$

The solution of this equation can be computed by using the Green’s function solution of the Poisson equation or, as in the present hybrid formulation, grid solvers.

The use of a mesh (M) conjointly with the particles (P) allows the use of efficient tools such as grid solvers and Finite Differences. This is demonstrated below in the case of a Euler time-step

- (P → M) Interpolate particle strengths on a lattice by evaluating Eq. 3 on grid locations

$$\boldsymbol{\omega}(\mathbf{x}_{ij\dots}) = \sum_p \boldsymbol{\alpha}_p \zeta^h(\mathbf{x}_{ij\dots} - \mathbf{x}_p) \quad (6)$$

where $\mathbf{x}_{ij\dots}$ is a grid node and $ij\dots$ are node indices

- (M → M) Perform operations on the grid, *i.e.* solve the Poisson equation for velocity in Fourier space, use Finite Differences and evaluate the right-hand sides of the system of Eq. 4
- (M → P) Interpolate velocities, right-hand sides, respectively back onto the particles,

$$\begin{aligned} \mathbf{u}(\mathbf{x}_p) &= \sum_i \sum_j \sum_{\dots} h^{-d} \mathbf{u}(\mathbf{x}_{ij\dots}) \zeta^h(\mathbf{x}_p - \mathbf{x}_{ij\dots}) \\ \frac{D\boldsymbol{\omega}}{Dt}(\mathbf{x}_p) &= \sum_i \sum_j \sum_{\dots} h^{-d} \frac{D\boldsymbol{\omega}}{Dt}(\mathbf{x}_{ij\dots}) \zeta^h(\mathbf{x}_p - \mathbf{x}_{ij\dots}) \end{aligned} \quad (7)$$

and advance the quantities and locations.

The Lagrangian distortion of the particles leads to loss of convergence[11, 12]. We ensure accuracy by means of a periodic reinitialization of the particle locations[13–16, 1]. This *remeshing* procedure, essentially a P → M interpolation, is performed at the end of every time step and uses the third order accurate M_4^1 kernel[17].

2.2 Implementation for parallel computer architectures

The method was implemented as a client application of the open source Parallel Particle Mesh (PPM) library[18]. PPM provides a general-purpose framework that can handle the simulation of particle-only, mesh-only or particle-mesh systems. The library defines topologies, *i.e.* space decompositions and the assignment of sub-domains to processors, which achieve particle- and mesh-based load balancing. The library provides several tools for the efficient parallelization of the particle-mesh approach described in Section 2.1. Data communication is organized in *local* and *global* mappings. Local mappings handle

- the advection of particles from a sub-domain into another
- ghost mesh points for the consistent summation of particle contributions along sub-domain boundaries, *e.g.* in the P → M step: the interpolation stencil will distribute particle strength to ghost points outside its own sub-domain

- ghost mesh points for consistent Finite Difference operations.

Global mappings are used for the transfer of mesh data from a topology to another, as in the case of the pencil topologies involved in multi-dimensional FFTs. PPM is written in Fortran 90 on top of the Message Passing Interface (MPI); the client uses the FFTW library[19] inside the Fourier solver.

The code is run on an IBM Blue Gene/L solution with dual cores nodes based on the PowerPC 440 700Mhz low power processor. Each node has 512MB of memory. The computations are all carried out in co-processor mode: one of the two CPUs is fully devoted to the communications. The machine used for production was the BG/L at IBM T.J. Watson Research Center - Yorktown Heights³ whereas porting, optimization and testing was done on the BG/L system of the IBM Zurich Research Laboratory. Machine dependent optimization consisted in

1. data reordering and compiler directives to exploit the double floating point unit of the PowerPC 440 processors,
2. mapping of the cartesian communicators to the BG/L torus,
3. use of the BG/L tree network for global reductions.

3 Aircraft wakes

The evolution and eventual destruction of the trailing vortices is affected by several types of instabilities, usually classified according to their wavelength. Long wavelength instabilities are the most powerful to drive the collapse of a vortex pair albeit with a slow growth rate. The well-known Crow instability[20] is an example of such instabilities that deforms the vortex lines into sinusoidal structures until vortices of opposite sign reconnect and form rings.

More complex systems with multiple vortex pairs can undergo other instabilities. A rapidly growing, medium-wavelength instability has been the focus of recent experimental [5, 7, 21] and numerical studies[8–10]. This instability occurs in the presence of a secondary vortex pair that is counter-rotating relative to the main pair. These secondary vortices are generated by a sufficient negative load on the horizontal tail or the inboard edge of outboard flaps. Being weaker, they eventually wrap around the primary ones in so-called Ω -loops, leading to the reconnection of vortices of unequal circulations. This in turn triggers an accelerated vortex destruction.

3.1 Convergence and scalability

We use the geometry of this particular medium wavelength instability to assess the performance of our code. The geometry of the problem is taken from [9]; it comprises two counter-rotating vortex pairs with spans b_1 , b_2 and circulations Γ_1 , Γ_2 . The Reynolds number is $Re = \Gamma_0/\nu = 3500$, where $\Gamma_0 = \Gamma_1 + \Gamma_2$. Three grid sizes were considered, $64 \times 320 \times 192$, $128 \times 640 \times 384$, and $256 \times$

³ Compiled with XLF version 10.1, with BG/L driver V1.3 and FFTW 3.1.1

1280 × 768, resulting in 4, 32 and 252 million particles respectively. All three configurations were run on 1024 processors of IBM BG/L. The time-step was kept constant for all resolutions $\Delta t = 3.3 \cdot 10^{-4} t_0$ where $t_0 = \frac{2\pi b_0^2}{\Gamma_0}$ and $b_0 = \frac{\Gamma_1 b_1 + \Gamma_2 b_2}{\Gamma_0}$. Figure 1 shows the evolution of vorticity iso-surfaces and the wrapping-around

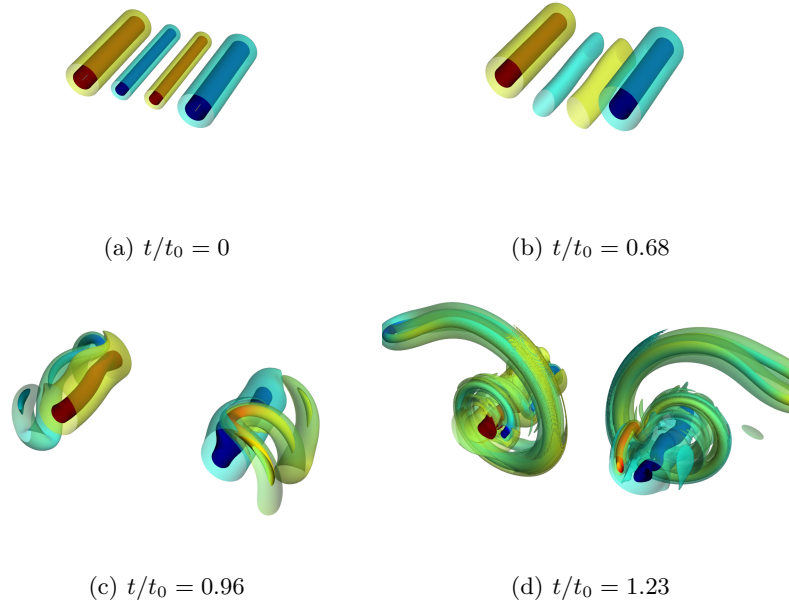


Fig. 1. Medium-wavelength instability of counter-rotating vortices, $128 \times 640 \times 384$ -grid: evolution of vorticity iso-surfaces. The opaque surface corresponds to $|\omega| = 10\Gamma_1/b_1^2$; the transparent one, to $|\omega| = 2\Gamma_1/b_1^2$.

of the secondary vortices around the main ones. Diagnostics (Fig. 2) such as the evolution of enstrophy, which measures the energy decay and the evolution of the effective numerical viscosity confirm the low dissipation of the method and its convergence.

The parallel scalability was assessed for $512 \leq N_{\text{CPU}} \leq 16384$ on IBM BG/L. We measure the strong efficiency as

$$\eta_{\text{strong}} = \frac{N_{\text{CPU}}^{\text{ref}} T(N_{\text{CPU}}^{\text{ref}})}{N_{\text{CPU}} T(N_{\text{CPU}})} \quad (8)$$

where T is the average computation time of one time step. In order to test the code up to the large sizes allowed by BG/L, we used $N_{\text{CPU}}^{\text{ref}} = 2048$ and a problem size of $768 \times 1024 \times 2048$ or 1.6 billion particles. This brings the

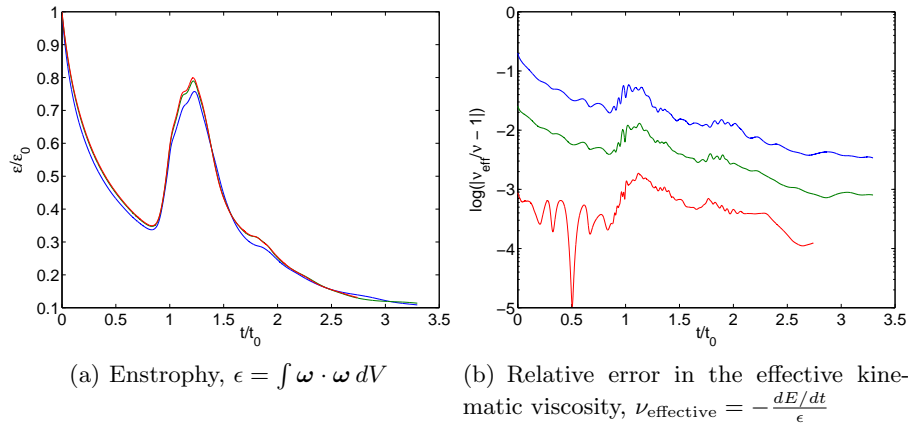


Fig. 2. Medium-wavelength instability of counter-rotating vortices: convergence and diagnostics for three spatial resolutions: $N_x = 64$ (blue), 128 (green) and 256 (red)

per-processor problem size from 786432 down to 98304 when we run on the maximum number of processors. The curve (Fig. 3(b)) displays a plateau up to $N_{\text{CPUS}} = 4096$, with the per-processor problem size becoming progressively smaller and communication overhead overwhelming the computing cycles.

From this result, we base our weak scalability study on a constant per-processor number of particles of $M_{\text{per CPU}} \simeq 4 \cdot 10^5$. We used the following measure

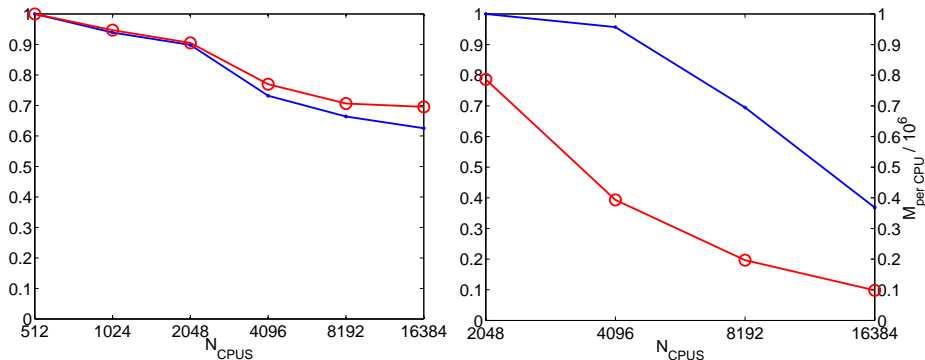
$$\eta_{\text{weak}} = \frac{T(N_{\text{CPUS}}^{\text{ref}}, M^{\text{ref}})}{T(N_{\text{CPUS}}, \frac{N_{\text{CPUS}}}{N_{\text{CPUS}}^{\text{ref}}} M^{\text{ref}})} \quad (9)$$

where we took $N_{\text{CPUS}}^{\text{ref}} = 512$. The code displays (Fig. 3(a)) excellent scalability up to $N_{\text{CPUS}} = 4096$. Eq. 9 assumes linear complexity for the problem at hand. There is however an $O(N \log N)$ component to the overall complexity of the present problem as we are solving the Poisson equation for the convection velocity. The two curves (with and without the cost for the solution of the Poisson equation) are shown in (Fig. 3(a)); the relatively small gap between the two curves manifests the good performance of the Poisson solver.

3.2 Instability initiation by ambient noise in a large domain

We consider the configuration presented in the state of the art calculations in [8, see configuration 2] simulating the onset of instabilities of multiple wavelengths in a long domain. The domain length is chosen as the wavelength of maximum growth rate for the Crow instability, $L_x = 9.4285b_1$. The transversal dimensions are $L_y = 1/2 L_x$ and $L_z = 3/8 L_x$. The vortices have Gaussian cores

$$\omega(r) = \frac{1}{2\pi\sigma^2} \exp(-(r/2\sigma)^2) \quad (10)$$



(a) Weak scalability for a per-processor (b) Strong scalability (solid dots) and per-processor size = $4 \cdot 10^5$; full problem (solid dots) and excluding the Poisson solver (circles)

Fig. 3. Medium-wavelength instability of counter-rotating vortices: parallel efficiencies on IBM BlueGene/L

with $\sigma_1/b_1 = 0.05$ and $\sigma_2/b_1 = 0.025$. The secondary pair is located at $b_2/b_1 = 0.5$, with a relative strength $\Gamma_2/\Gamma_1 = -0.35$. In addition to the initially unperturbed vortices, the vorticity field is filled with a white noise that produces $u_{\text{RMS}} = 0.005 u_{\text{max}}$. We study this flow with DNS at $Re_{\Gamma_1} = 6000$. This represents a three-fold increase over previously reported Reynolds numbers [8]. In addition, these prior simulations used a coarse resolution and a crude LES model (MILES[22]) to model the high Reynolds number dynamics of the flow. The present DNS is afforded due to a mesh resolution of $2048 \times 1024 \times 768$ and 1.6 billion particles. It is run on 4096 CPUs; the wall-clock computation time was 39s on average per time step. With approximately 10000 time steps, this represents a time-to-solution of 100 hours.

Figure 4 shows that this system with a random initial condition picks up the medium-wavelength instability. At $t/t_0 = 0.25$ (Fig. 4(b)), we count 10 and 11 Ω -loops along the two primary vortices. This corresponds to the average wavelengths $\lambda/b_1 = 0.943$ and 0.86 . These values are sensibly different from the ones reported in [8], 1.047 and 1.309. This comparison, however, considers the problem at the end of the exponential growth and ignores the uneven distribution of loop wavelengths and hence, individual growth rates.

4 Vortex rings

The same code has been applied to the turbulent decay of vortex rings at $Re_{\Gamma} = 7500$ [23]. It allowed the analysis of the vortex dynamics in the non-linear stage and their correlation with structures captured in dye visualization and

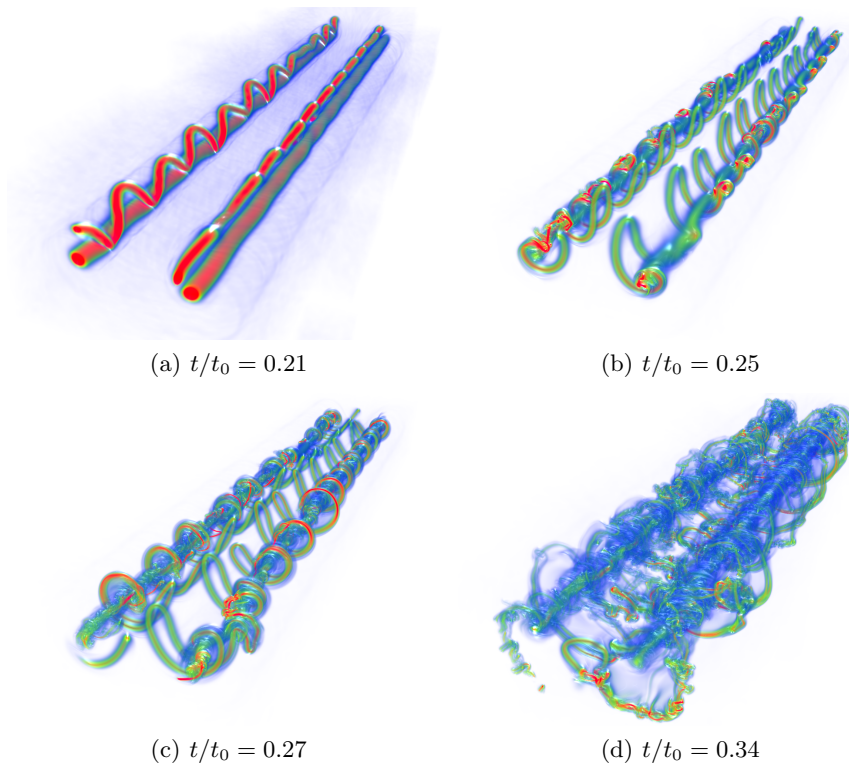


Fig. 4. Counter-rotating vortices, initiation by ambient noise: visualization of the vorticity structures by volume rendering. High vorticity norm regions correspond to red and opaque; low vorticity are blue and transparent.

an observed decay of circulation. Figure 5 shows the emergence of stream-wise structures in the ring.

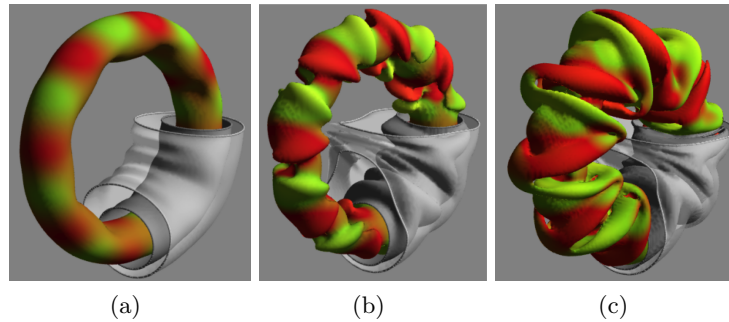


Fig. 5. Evolution of a Vortex ring at $Re=7500$: vorticity iso-surfaces colored by the stream-wise component of vorticity.

5 Conclusions

This paper presents the implementation of an efficient particle-mesh method for massively parallel architectures and its application to wakes. We refer to [24] for a more extensive assessment of the method.

Our code displays good scalability up to $16K$ processors on BlueGene/L. The origin of the parallel efficiency drop at $4K$ is being investigated; a possible cause is the recurrent computation of mesh intersections inside the global mappings. Other code development efforts include the implementation of unbounded boundary conditions based on fast convolutions in Fourier space[25] and non-periodic conditions in the axial direction. Finally, the optimization of vortex dynamics for enhanced decay and mixing is the subject of ongoing investigations.

References

1. Winckelmans, G.: Vortex methods. In Stein, E., De Borst, R., Hughes, T.J., eds.: Encyclopedia of Computational Mechanics. Volume 3. John Wiley and Sons (2004)
2. Koumoutsakos, P.: Multiscale flow simulations using particles. *Annu. Rev. Fluid Mech.* **37** (2005) 457–487
3. Crouch, J.D.: Instability and transient growth for two trailing-vortex pairs. *Journal of Fluid Mechanics* **350** (1997) 311–330
4. Crouch, J.D., Miller, G.D., Spalart, P.R.: Active-control system for breakup of airplane trailing vortices. *AIAA Journal* **39**(12) (Dec 2001) 2374–2381
5. Durston, D.A., Walker, S.M., Driver, D.M., Smith, S.C., Savas, Ö.: Wake vortex alleviation flow field studies. *J. Aircraft* **42**(4) (2005) 894–907

6. Graham, W.R., Park, S.W., Nickels, T.B.: Trailing vortices from a wing with a notched lift distribution. *AIAA Journal* **41**(9) (2003) 1835–1838
7. Ortega, J.M., Savas, Ö.: Rapidly growing instability mode in trailing multiple-vortex wakes. *AIAA Journal* **39**(4) (2001) 750–754
8. Stumpf, E.: Study of four-vortex aircraft wakes and layout of corresponding aircraft configurations. *J. Aircraft* **42**(3) (2005) 722–730
9. Winckelmans, G., Cocle, R., Dufresne, L., Capart, R.: Vortex methods and their application to trailing wake vortex simulations. *C. R. Phys.* **6**(4-5) (2005) 467–486
10. Cocle, R., Dufresne, L., Winckelmans, G.: Investigation of multiscale subgrid models for les of instabilities and turbulence in wake vortex systems. *Lecture Notes in Computational Science and Engineering* **56** (2007)
11. Beale, J.T., Majda, A.: Vortex methods I: convergence in 3 dimensions. *Mathematics of Computation* **39**(159) (1982) 1–27
12. Beale, J.T.: On the accuracy of vortex methods at large times. In et al., B.E., ed.: *Proc. Workshop on Comput. Fluid Dyn. and React. Gas Flows*, IMA, Univ. of Minnesota, 1986, Springer-Verlag, New York (1988) 19
13. Cottet, G.H.: Artificial viscosity models for vortex and particle methods. *J. Comput. Phys.* **127**(2) (1996) 299–308
14. Koumoutsakos, P.: Inviscid axisymmetrization of an elliptical vortex. *J. Comput. Phys.* **138**(2) (1997) 821–857
15. Chaniotis, A., Poulidakos, D., Koumoutsakos, P.: Remeshed smoothed particle hydrodynamics for the simulation of viscous and heat conducting flows. *J. Comput. Phys.* **182** (2002) 67–90
16. Eldredge, J.D., Colonius, T., Leonard, A.: A vortex particle method for two dimensional compressible flow. *J. Comp. Phys.* **179** (2002) 371–399
17. Monaghan, J.J.: Extrapolating b splines for interpolation;. *Journal of Computational Physics* **60**(2) (1985) 253–262
18. Sbalzarini, I.F., Walther, J.H., Bergdorf, M., Hieber, S.E., Kotsalis, E.M., Koumoutsakos, P.: PPM a highly efficient parallel particle mesh library for the simulation of continuum systems. *J. Comput. Phys.* **215** (July 2006) 566–588
19. Frigo, M., Johnson, S.G.: FFTW: An adaptive software architecture for the FFT. In: *Proc. IEEE Intl. Conf. on Acoustics, Speech, and Signal Processing*. Volume 3., Seattle, WA (May 1998) 1381–1384
20. Crow, S.C.: Stability theory for a pair of trailing vortices. *AIAA Journal* **8**(12) (1970) 2172–2179
21. Stuff, R.: The near-far relationship of vortices shed from transport aircraft. In AIAA, ed.: *AIAA Applied Aerodynamics Conference*, 19th, Anaheim, CA, AIAA (2001) AIAA–2001–2429
22. Boris, J.P., Grinstein, F.F., Oran, E.S., Kolbe, R.L.: New insights into large eddy simulation. *Fluid Dynamics Research* **10**(4-6) (Dec 1992) 199–228
23. Bergdorf, M., Koumoutsakos, P., Leonard, A.: Direct numerical simulations of vortex rings at $re_\gamma = 7500$. *J. Fluid. Mech.* **581** (2007) 495–505
24. Chatelain, P., Curioni, A., Bergdorf, M., Rossinelli, D., Andreoni, W., Koumoutsakos, P.: Billion vortex particle direct numerical simulations of aircraft wakes. *Computer Methods in Applied Mechanics and Engineering* **197**(13) (Feb 2008) 1296–1304
25. Hockney, R., Eastwood, J.: *Computer Simulation using Particles*. Institute of Physics Publishing (1988)